ACS OMEGA

http://pubs.acs.org/journal/acsodf

Article

Adsorption of Phosgene Gas on Pristine and Copper-Decorated $B_{12}N_{12}$ Nanocages: A Comparative DFT Study

Shahid Hussain, Riaz Hussain, Muhammad Yasir Mehboob, Shahzad Ali Shahid Chatha, Abdullah Ijaz Hussain, Ali Umar, Muhammad Usman Khan, Mahmood Ahmed, Muhammad Adnan, and Khurshid Ayub*

Cite This: *ACS Omega* 2020, 5, 7641−7650

Read Online

ACCESS | Metrics & More | Article Recommendations | Supporting Information

ABSTRACT: Nanostructured gas sensors find diverse applications in environmental and agricultural monitoring. Herein, adsorption of phosgene ($COCl_2$) on pure and copper-decorated $B_{12}N_{12}$ (Cu−BN) is analyzed through density functional theory (DFT) calculations. Adsorption of copper on $B_{12}N_{12}$ results in two optimized geometries, named Cu@b_{66} and Cu@b_{64}, with adsorption energies of −193.81 and −198.45 kJ/mol, respectively. The adsorption/interaction energies of $COCl_2$ on pure BN nanocages are −9.30, −6.90, and −3.70 kJ/mol in **G1**, **G2**, and **G3** geometries, respectively, whereas the interaction energies of $COCl_2$ on copper-decorated BN are −1.66 and −16.95 kJ/mol for **B1** and **B2**, respectively. To examine the changes in the properties of pure and Cu−BN nanocages, geometric parameters, dipole moment, Q_{NBO}, frontier molecular orbitals, and partial density of states (PDOS) are analyzed to comprehensively illustrate the interaction mechanism. The results of these parameters reveal that $COCl_2$ binds more strongly onto copper-doped BN nanocages. Moreover, a higher charge separation is observed in $COCl_2$−Cu−BN geometries as compared to copper-decorated BN geometries. Therefore, these nanocages may be considered as potential candidates for application in phosgene sensors.

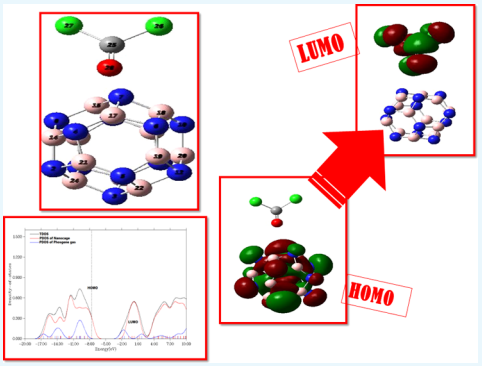

1. INTRODUCTION

The field of nanotechnology and nanoscience has developed rapidly. Discovery of nanotubes (carbon nanotubes) by Ijimia increased the demand for nanoscale materials and laid the foundation for the rapid development of the field of nanoscale materials (carbon nanoscale materials).[1] Nanomaterials such as nanocages, nanoclusters, and nanotubes find vast applications in optical devices,[2,3] catalysis,[4] sensing materials (sensors),[5] adsorption,[6,7] and medical[8] and electronic devices.[9]

Besides the use of carbon nanotubes and fullerene (C_{60}) in advanced devices, extensive efforts have been made toward the synthesis of tubular or spherical fullerenes of diverse inorganic (non-carbon) materials over the last several years. Boron nitride (BN),[10,11] silica,[12] and aluminum nitride (AlN) nanotubes and co-axial cubic AlN−BN composites[13] are the most important and interesting examples in this regard. Due to the closed electronic shells of nanoclusters, they are considered to be very stable and play a vital role in the development of materials used in advanced technologies. Therefore, they are the subject of several investigations.[14] Studies illustrate that $(XY)_n$ clusters, $X_{12}Y_{12}$ (X = Al, B, Ga and Y = As, N, P), are the most stable (magic clusters).[15,16] Toftlund and Jensen reported different geometries of B_XN_Y nanoclusters in their reports and concluded that the $B_{12}N_{12}$ nanocluster is highly stable and important as compared to C24.[15] These III−V clusters also find applications in light-emitting diodes and microelectronic devices.[17,18] $B_{12}N_{12}$ and $A_{12}N_{12}$ (two semiconductor-like group III−V clusters) have excellent physiochemical properties.[19,20]

Boron nitrides $(BN)_x$ have drawn attention due to their large thermal conductivity, large highest occupied molecular orbital−lowest unoccupied molecular orbital (HOMO−LUMO) gap, high temperature stability, low dielectric constant, and high resistance to oxidation.[21−23] Oku et al. synthesized $B_{12}N_{12}$ nanocages, which consist of eight hexagonal rings and six tetragonal rings.[22] Moreover, the phenomenon of charge separation occurs between boron (B) and nitrogen (N), where the boron atom acts as an electron-deficient (Lewis acid) and the nitrogen atom acts as an electron-rich species (Lewis base). Due to this concept, the BN nanostructure is considered to behave as a noncatalyst (as it is a Lewis acid−Lewis base pair).

Recently, studies of the interaction of pure $B_{12}N_{12}$ nanoclusters with different systems, such as methylamine,[24]

Received: February 5, 2020
Accepted: March 6, 2020
Published: March 26, 2020

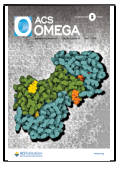

https://dx.doi.org/10.1021/acsomega.0c00507
ACS Omega 2020, 5, 7641−7650

CO_2,[25] CO,[26] NO, hydrogen, N_2, methane,[27] mono-fluoromethane (MFM), thiophene,[28] mono-chloromethane (MCM),[29] SO_2, and O_3,[30] using density functional theory (DFT) have been reported. Similar intermolecular interactions are also part of valuable literature in which interactions between different molecules were studied.[31−33] Similarly, the noncovalent interaction among halide ion complexes in decaborane was also studied for elaborating different noncovalent interactions.[34] The interaction and dissociative reactions of CH_3−OH on $B_{12}N_{12}$ nanocages are also studied.[35] Adsorption of biological molecules, such as cytosine, adenine, and uracil, on $B_{12}N_{12}$ nanoclusters was investigated.[36] Further, biological molecules, such as guanine, are also adsorbed on $X_{12}Y_{12}$ nanocages.[37] Adsorption of SCN^- on pure and Mg^--, Al^--, and Si-doped BN ($B_{12}N_{12}$ and $B_{16}N_{16}$) nanocages was reported.[38] Recently, adsorption of hydrogen molecules on nickel-decorated $B_{12}N_{12}$[39] was reported. Moreover, adsorption of pyrrole on $Al_{12}N_{12}$, $Al_{12}P_{12}$, $B_{12}N_{12}$, and $B_{12}P_{12}$ was also reported previously.[40] Other than adsorption, BN fullerenes find applications in storage materials,[41−44] field-effect transistors,[45] nonlinear optics,[46,47] and magnetic nanoparticles.[48] Recently, researchers disclosed the superatomic nature of BN nanocages.[49] Moreover, diffusion of alkali metals has been studied on boron nitride fullerenes to evaluate their potential applications in batteries.[50,51]

Phosgene ($COCl_2$), being the simplest acid chloride, is a colorless gas and is formally derived from carbonic acid. It is mainly used in industries (polyurethane industry) to produce polymeric isocyanates and in the preparation of carbamates, pharmaceuticals, and related pesticides. It is the building block of many organic compounds, dyes, and isocyanates and finds useful applications as a reagent in several industries. It is also called a chemical war weapon (highly toxic gas) used in World War I (as a chemical weapon). Exposure to phosgene may result in swelling of throat, change in voice, pulmonary irritation, or delayed pulmonary edema.[52] For this reason, it is necessary to detect phosgene and remove it from air even when present at very small concentrations. The adsorption of phosgene gas with various surfaces, such as AlN nanotubes,[53] charcoal surface,[54] and TiO_2,[55] has been investigated. Phosgene detection by Sc-doped BN nanotubes was reported.[56] Moreover, the interaction of phosgene gas ($COCl_2$) with Ga-doped and Al-doped BN ($B_{16}N_{16}$ and $B_{12}N_{12}$) nanoclusters was reported by Shakerzadeh et al.[57] Their study revealed that the interaction of phosgene gas with Al- and Ga-doped nanoclusters caused a reduction in the HOMO−LUMO gap. Using DFT calculations, the adsorption of phosgene on $(XY)_n$ (X = Al, B and Y = P, N) was also reported by Padash et al.[58]

Despite these advances, adsorption of phosgene on late transition metal (such as copper)-doped $B_{12}N_{12}$ fullerene has not yet been reported. Early transition metals bind too tightly to be detached from the surface at the end. On the other hand, late transition metals bind with these surfaces with reasonable affinity. A number of reports have already been published on nickel decoration in the literature, whereas copper-decorated surfaces are not well explored. A recent report in the literature illustrated that copper effectively binds with BN nanocages.[59] Moreover, copper is generally not poisoned by analytes, whereas nickel is poisoned to some extent, particularly by sulfur-containing analytes.[60−62] Copper also has good tendency to adsorb various oxygen-containing analytes. Therefore, all of these findings motivated us to design a system that efficiently binds the highly toxic $COCl_2$ gas by structural modification (i.e., decoration of Cu metal on BN) and help in removing this dangerous gas from the environment. The decoration of nanostructures with metals is much preferred over doping (where an atom of the nanostructure is replaced with an external atom). For doping, a defect may be created, which can impart certain interesting properties but, at the same time, render the system unstable in terms of binding energies (low binding energies). On the other hand, decoration does not disturb the intrinsic stability of the systems.[30,63,64] Moreover, the metal atoms can be easily detached from the nanostructure as and when required. These characteristics motivated us to study decoration rather than doping with metal atoms. In this study, we examined phosgene adsorption on pure BN and Cu-doped BN nanocages. First, we explored the electronic and geometric properties of the $B_{12}N_{12}$ surface upon adsorption of Cu metal through interaction energies, dipole moment, Q_{NBO} (charge), frontier molecular orbital analysis (HOMO and LUMO), and partial density of states (PDOS). Then, the interaction of phosgene gas with optimized structures of copper-decorated BN was investigated.

2. COMPUTATIONAL METHODOLOGY

All calculations in this study were performed at the B3LYP/6-31G (d,p) level of theory using Gaussian 09.[65] Geometry optimization, adsorption energies, dipole moment, charge transfer (Q_{NBO}), molecular electrostatic potential (MEP), frontier molecular orbitals (HOMO−LUMO distribution), and partial density of states (PDOS) were calculated to study the interaction mechanism. B3LYP/6-31G (d,p) is a reliable level of theory, which is frequently used for nanoclusters.[39,46,66] Geometries are optimized without any symmetry constraints in different spin states with zero net charge on the complexes. The doublet spin state is the lowest energy spin state for copper-containing systems. Many different possible orientations of copper on the BN nanocage (M@b_{66}, M@b_{64}, M@R_6, M@R_4, M@B_{top}, and M@N_{top}) were considered for optimization, but all above-mentioned input geometries converged into two optimized structures, which we named **A1**(M@b_{66}) and **A2** (M@b_{64}).

Equation 1 is used to calculate the interaction or adsorption energy of Cu on the BN nanocage in three positions.

$$E_{ad} = E_{Cu-BN} - (E_{BN} + E_{Cu}) \quad (1)$$

where E_{Cu-BN} stands for the energy of the Cu−BN nanocage complex. E_{BN} stands for the total energy of the pure BN nanocage, and E_{Cu} describes the electronic energy of Cu.

Equations 2 and 3 are used to calculate the interaction or adsorption energies of $COCl_2$ with the pure BN nanocage and copper-decorated BN nanocage.

$$E_{ad(BN)} = E_{COCl_2-BN} - (E_{BN} + E_{COCl_2}) \quad (2)$$

$$E_{ad(Cu-BN)} = E_{COCl_2-Cu-BN} - (E_{Cu-BN} - E_{COCl_2}) \quad (3)$$

Here, $E_{int(BN)}$ and $E_{int(Cu-BN)}$ represent the interaction/adsorption energy of phosgene with the BN nanocage and Cu-decorated BN, respectively. $E_{phosgene-BN}$ and $E_{phosgene-Cu-BN}$ represent the total electronic energies of the $COCl_2$−BN nanocage complex and $COCl_2$−copper-decorated BN nanocage. $E_{phosgene}$ stands for the total energy of single $COCl_2$.

Parr et al.[67] in 1999 studied the chemical potential (μ) and expressed it by the following eq 4.

https://dx.doi.org/10.1021/acsomega.0c00507
ACS Omega 2020, 5, 7641−7650

$$\mu = -(I + A)/2 \quad (4)$$

E_{HOMO} represents the energy of the HOMO, and E_{LUMO} represents the energy of the LUMO. Moreover, properties such as softness (S), hardness (η), and electrophilicity (ω) can be determined using the Koopmans theorem.[68]

$$\eta = (I - A)/2 \quad (5)$$

$$S = 1/(2\eta) \quad (6)$$

$$\omega = \mu^2/2\eta \quad (7)$$

Partial density of states (PDOS) diagrams for all systems are generated using MultiWFN software.[69]

3. RESULTS AND DISCUSSION

3.1. Bond Length and Adsorption Energies. The BN optimized structure at the B3LYP/6-31G (d,p) basis set is shown in Figure 1. The BN cluster is quite stable as the nitrogen and boron sites in this cluster are equivalent. The cluster consists of six tetragonal (4-membered) and eight hexagonal (6-membered) rings. The B−N bond length varies depending on the position whether the bond is between a tetragonal and a hexagonal ring (b_{64}) or between two hexagonal rings (b_{66}). The B−N bond length shared between two hexagonal rings (b_{66}) is 1.44 Å, whereas the B−N bond length shared between a tetragonal and a hexagonal ring (b_{64}) is 1.49 Å.

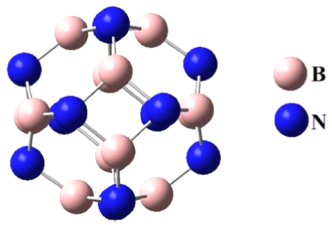

Figure 1. Optimized structure of $B_{12}N_{12}$.

For decoration of copper on the BN nanocage, one finds several positions on which copper shows an interaction with rings. These positions may be M@B_{top}, M@N_{top}, M@R_6 (metal on the hexagonal ring), M@R_4 (metal on the tetragonal ring), M@b_{64} (metal on the bond present between a 6- and a 4-membered ring), and M@b_{66} (metal on the bond present between two hexagonal rings). All possible input geometries were directed for optimization; however, only two geometries could be obtained, named **A1** and **A2**, because all above-mentioned initial inputs converged merely into these two geometries after optimization. In these geometries, one is M@b_{66} named **A1**, whereas the other is M@b_{64} named **A2**.

In general, copper decoration on the BN cage causes changes in the geometry of the BN cage. When Cu (metal) is present on the bond present between two hexagonal rings (**A1**), the B−N bond length is elongated to 1.55 Å (as compared to 1.44 Å in the pure BN cage). The adsorption energy in this geometry (**A1**) is −193.81 kJ/mol. Moreover, the N−Cu and B−Cu bond lengths are 1.95 and 1.92 Å, respectively in the **A1** geometry. In the same way, adsorption of Cu (metal) on the bond present between one hexagonal and one tetragonal ring (M@b_{64}) in the **A2** geometry causes an elongation of the B−N bond length to 1.66 Å (as compared to 1.49 Å in the pure cage). Furthermore, the B−Cu bond length increases to 1.94 Å as compared to 1.92 Å in **A1**, but the N−Cu bond length is shortened to 1.94 Å as compared to 1.95 Å in **A1**. The adsorption energy in the **A2** geometry (198.45 kJ/mol) is higher than that in the **A1** geometry. These two geometries are represented in Figure 2.

Then, we analyzed the interaction of phosgene ($COCl_2$) gas with the pristine BN cage. Different orientations of $COCl_2$ gas were studied on the pristine BN cage. As a result, we got three different geometries with respect to the orientation of $COCl_2$ on the $B_{12}N_{12}$ nanocage. These geometries are named **G1, G2**, and **G3** (Figure 3). In all orientations, carbonyl oxygen is oriented toward BN nanocages, but the orientation of $COCl_2$ on $B_{12}N_{12}$ nanocages is different (Figure 3) in each case. In **G1** and **G2** orientations, $COCl_2$ is oriented at distances of 2.62 and 2.85 Å, respectively, to the nearest atom on the cage with adsorption energies of −9.43 and −6.90 kJ/mol, respectively (Figure 3). In the **G3** geometry, the value of bond length between $COCl_2$ and the BN cage is 3.26 Å, as the gas is situated in the center of the ring in the relaxed structure, while adsorption energy in this case is −3.70 kJ/mol. This change in adsorption energies is due to the increase in the distance of oxygen (of the carbonyl group of phosgene gas) from the BN nanocage because strong adsorptions are observed at short distances (as in **G1** and **G2**). From the data, it is obvious that $COCl_2$ is not favorably adsorbed on the pristine BN cage due to the small value of the adsorption energy in all three cases. The most stable structure among the three was **G1**, which had a higher adsorption energy compared to **G2** and **G3**, but the overall weak interactions of $COCl_2$ with BN were observed.

Furthermore, the adsorption of $COCl_2$ on the copper-decorated BN nanocage was studied. Adsorption of phosgene on the **A1** geometry resulted in the **B1** geometry, where phosgene gas was physisorbed. The observed bond length between the nearest atom of $COCl_2$ gas ("Cl" in **B1**) and the Cu−BN cage for **B1** was 4.17 Å with an adsorption energy of −1.66 kJ/mol. Moreover, $COCl_2$ does not elongate the B−N bond length (1.55 Å) in the **B1** geometry mainly because it exhibits a weak physisorption.

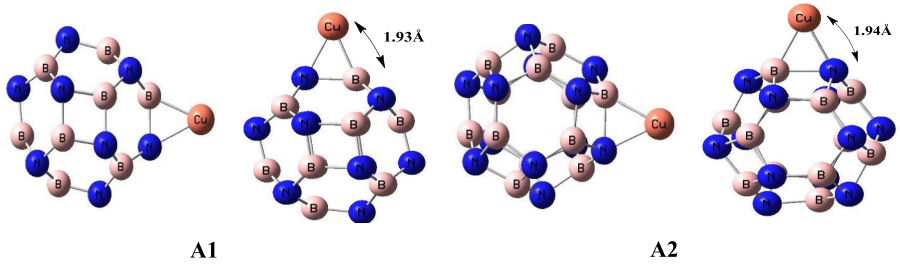

Figure 2. Optimized structures of Cu-doped $B_{12}N_{12}$ nanocages.

https://dx.doi.org/10.1021/acsomega.0c00507
ACS Omega 2020, 5, 7641−7650

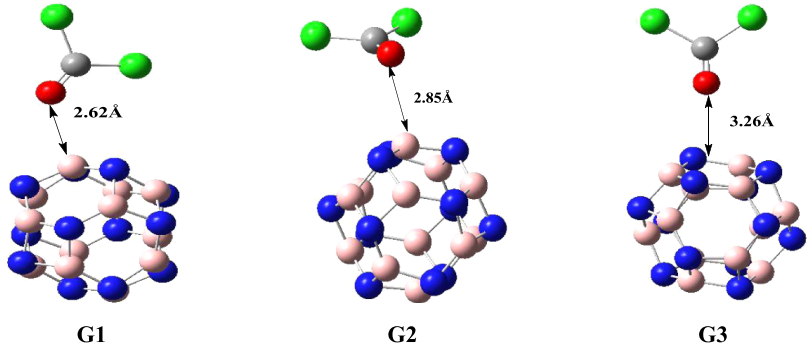

Figure 3. Different orientations of $COCl_2$ on BN. In the **G3** orientation, $COCl_2$ is situated in the center of the ring, so the average distance is calculated.

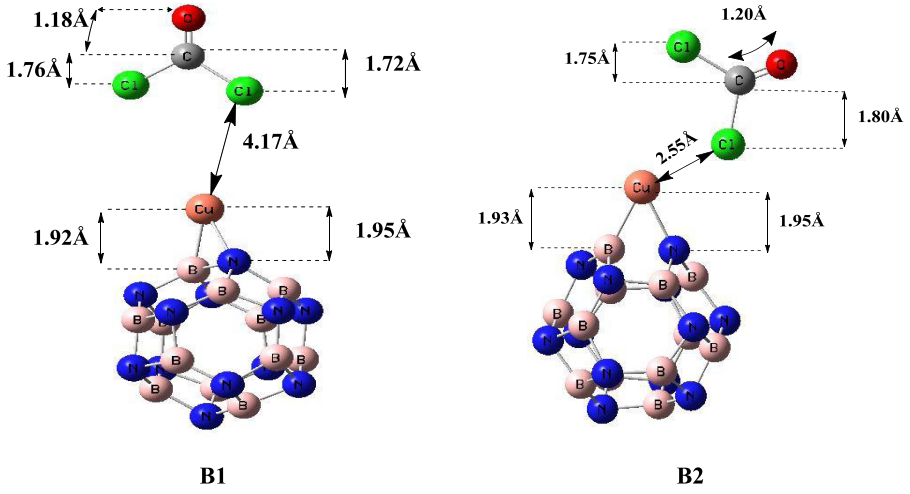

Figure 4. Optimized structures of $COCl_2$-adsorbed $Cu-B_{12}N_{12}$.

Likewise, adsorption of $COCl_2$ on **A2** (Cu−BN) also resulted in a geometry named **B2**. The bond length between the nearest atom of gas ("Cl" in **B2**) and the Cu−BN cage was 2.55 Å with an adsorption energy of −16.95 kJ/mol. Comparing both orientations (**B1** and **B2**), it is obvious that **B2** is a more stable orientation than **B1** because of its high adsorption energy. This quite strong interaction of $COCl_2$ is also verified by the interaction distance of $COCl_2$ from Cu. Adsorption of $COCl_2$ on Cu−BN (**A2**) also causes an elongation of B−N bond lengths (1.67−1.70 Å in **B2**).

It is apparent that the adsorption of $COCl_2$ on the BN nanocage not only changes the Cu−BN distances but also changes the B−N bond lengths of Cu−BN. Small variations in N−Cu and B−Cu bond lengths were noticed after adsorption of $COCl_2$ on Cu−BN. So, from the above discussion, it is clear that $COCl_2$ is favorably adsorbed on Cu-doped $B_{12}N_{12}$ (**B2**) as compared to pure $B_{12}N_{12}$ (**G1, G2**, and **G3**).

3.2. Dipole Moment. The change in the dipole moments of pure BN, Cu-decorated BN, and $COCl_2$−Cu−BN was analyzed. The pure BN cage shows zero dipole moment as it is a symmetrical structure. Placement of Cu on this BN cage increases the dipole moment value from zero to 1.72 D in **A1** and 1.49 D in **A2**. These changes are attributed to the placement of the Cu metal, which disturbs the charge separation in BN nanocages. In **A1** and **A2** geometries, the dipole moment vectors are pointed toward the BN nanocage. Moreover, the change in dipole moment was analyzed after adsorption of phosgene gas on BN. The dipole moment vectors in **G1, G2**, and **G3** pointed toward $COCl_2$, which evidenced the charge transfer from $COCl_2$ to the nanocage, as shown in Figure S1 (Supporting Information). The values of dipole moment are 2.09, 1.36, and 1.54 D in **G1, G2**, and **G3**, respectively. The range of dipole moments is between 3.72 and 1.30 D for $COCl_2$-adsorbed Cu@BN nanocages. After adsorption of $COCl_2$ on Cu-decorated BN nanocages, the change in dipole moment originates due to charge transfer from the metal to phosgene gas. A comparison between **B1** and **B2** geometries illustrates a higher charge separation value in **B2** due to higher charge transfer.

The highest change in dipole moment is observed when $COCl_2$ complexes with $Cu-B_{12}N_{12}$ (**B2**), whereas the lowest dipole moment is calculated for **B1** ($COCl_2-Cu-B_{12}N_{12}$). In the **B2** geometry, significant charge transfer occurs when $COCl_2$ interacts with Cu-decorated BN (vide infra). On the hand, insignificant charge transfer is noticed in the **B1** orientation. The dipole moment depends on the quantity of charges as well as their separation. Less intense charges on **B1** are responsible for its low dipole moment among all geometries (vide infra). Moreover, the distance between $COCl_2$ and Cu−BN is large in **B1** as compared to other geometries, which is also another reason for its low dipole moment. The direction of the dipole moment vector is important in this regard; therefore, the dipole moment vector for all systems is given in the Supporting Information (Figure S1). The decreasing order of dipole moment is **B2** > **G1** > **A1** > **G3** > **A2** > **G2** > **B1**. This order specifies the maximum and

https://dx.doi.org/10.1021/acsomega.0c00507
ACS Omega 2020, 5, 7641−7650

Table 1. Closest Distance of Cu to $B_{12}N_{12}$, $COCl_2$ to Pure $B_{12}N_{12}$, and $COCl_2$ to Cu−BN, Q_{NBO} on the Metal and Gas ($COCl_2$), Dipole Moment, and Adsorption Energies of Different Systems

systems	d_{Cu-BN} (Å)	d_{COCl_2-Cu} (Å)	Q_{NBO} on $COCl_2$ (e)	Q_{NBO} on Cu (e)	μ_D (Debye)	E_{ad}(kJ/mol)
Cu				0.00	0.00	
BN					0.00	
BN−$COCl_2$ (**G1**)		2.62	0.05		2.09	−9.43
BN−$COCl_2$ (**G2**)		2.85	0.02		1.36	−6.90
BN−$COCl_2$ (**G3**)		3.26	0.004		1.54	−3.70
Cu−BN (**A1**)	1.93			0.517	1.72	−193.81
Cu−BN−$COCl_2$ (**B1**)	1.93	4.17	0.015	0.513	1.30	−1.66
Cu−BN (**A2**)	1.94			0.540	1.49	−198.45
Cu−BN−$COCl_2$ (**B2**)	1.94	2.55	0.062	0.591	3.72	−16.95

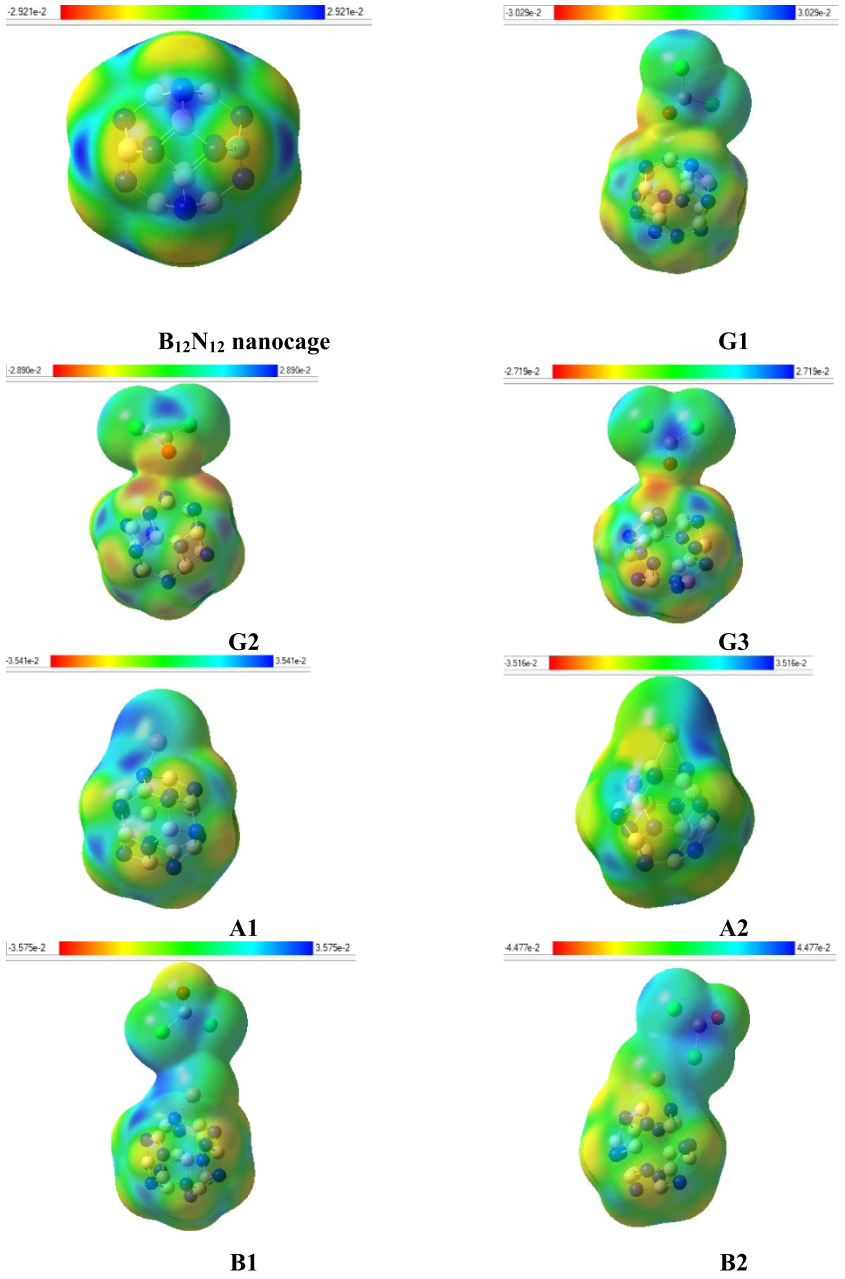

Figure 5. MEP of different systems (for understanding the color in these figures, the reader must read the web version of this article). The isosurface value is 0.02 e/Å^3.

minimum extremes of charge separation and dipole moment in all geometries Figure 4.

3.3. Q_{NBO}. Q_{NBO} was performed to rationalize the change in dipole moment after adsorption of Cu on the BN nanocage

https://dx.doi.org/10.1021/acsomega.0c00507
ACS Omega 2020, 5, 7641−7650

and that of $COCl_2$ on pure and Cu-decorated BN nanocages. The values of Q_{NBO} on Cu in **A1** and **A2** are 0.517 and 0.540, respectively. The Q_{NBO} on the metal is further increased after the adsorption of $COCl_2$ on Cu-decorated BN except for the **B1** geometry. The values of Q_{NBO} for these geometries are 0.513 (**B1**) and 0.591 (**B2**). The Q_{NBO} on the metal after adsorption of $COCl_2$ on Cu−BN varies among different geometries due to the interaction of $COCl_2$. With the increase in dipole moment, the Q_{NBO} on the metal also increases except in the **B1** geometry, in which the dipole moment decreases resulting in a decrease in Q_{NBO}. So, a regular change is observed in Q_{NBO} with the change in dipole moment for $COCl_2$-adsorbed Cu−BN nanocages (**B2**), as shown in Table 1.

3.4. MEP Analysis. The molecular electrostatic potential (MEP) is used to comprehend the interaction between the components of Cu−BN, $COCl_2$−BN, and Cu−BN−$COCl_2$ nanocages. It signifies the extent of charge distribution in a molecule and correlates the molecular structure with physiochemical properties, i.e., chemical reactivity, dipole moment, and partial charges. In Figure 5, the electron deficient blue area (in the web version) specifies boron atoms, while electron rich yellow region represent nitrogen atoms. The pure BN cage, being symmetrical, shows both the charges to an equal extent, which vary slightly after the adsorption of $COCl_2$ on the pure BN cage (**G1**, **G2**, and **G3**). The adsorption of $COCl_2$ decreases the intensity of the blue region on the BN nanocage (shifting toward $COCl_2$).

However, after the decoration of Cu on the pure BN cage, the blue area is shifted on top of the Cu metal, whereas the yellow area in the cage becomes less intense. This change can be seen in **A1** and **A2**. After the adsorption of $COCl_2$ on Cu-decorated BN nanocages (**B1** and **B2**), the blue area is shifted to the vicinity of the metal and the yellow color is regenerated on the cage (Figure 5). All this color shifting (charges) is attributed to an increase in dipole moment (D). For instance, pure BN has zero dipole moment, while Cu-decorated BN has some value of dipole moment.

3.5. Electronic Properties. Densities and electronic energy levels give a clear illustration of the effect of Cu decoration and $COCl_2$ adsorption on pure and Cu-doped $B_{12}N_{12}$ nanocages. Some orbital parameters, such as energies of the HOMO and LUMO, Fermi level (E_{FL}), and HOMO−LUMO band gap (E_g), are given in Table 2. The $B_{12}N_{12}$ nanocage is a semiconductor, which possesses a HOMO−LUMO gap (E_g) value of 6.84 eV. The HOMO and LUMO energies of the BN nanocage are −7.71 and −0.87 eV, respectively. The Fermi level, E_{FL}, value is −4.29 eV. The Fermi level designates the midpoint of the HOMO−LUMO energy gap (in a molecule when the temperature is 0 K). The placement of Cu on the BN nanocage changes the HOMO−LUMO energies. For the **A1** geometry, the energy of the HOMO is increased (−4.58 eV) but that of the LUMO is decreased (−1.72 eV). The HOMO−LUMO gap is also narrow (3.13 eV), and the Fermi level is positioned at −3.29 eV. For the **A2** geometry, an increased value of HOMO energy is observed (−4.89 eV), while the energy of the LUMO is decreased (−1.83 eV), which results in a decrease in the HOMO−LUMO gap (3.05 eV). Moreover, the Fermi level is positioned at −3.36 eV. This change in energies of the HOMO and LUMO is attributed to the stabilization and destabilization of the LUMO and HOMO, respectively.

To justify these differences, the shapes of frontier orbitals are evaluated (Figure 6). In general, the adsorption of Cu on BN nanocages results in a shift of the HOMO to the copper metal. This happens due to the presence of many electronegative atoms that make the metal atom electron rich. The metal, being electropositive, cannot retain these electrons, and therefore, they are spread out as excess electrons.

Table 2. Orbital Parameters: HOMO and LUMO Energies, Fermi Level, HOMO−LUMO Energy Gap for Different Systems

system	E_{HOMO} (eV)	E_{FL} (eV)	E_{LUMO} (eV)	E_g (eV)
Cu	−5.98	−3.32	−0.67	5.30
BN	−7.71	−4.29	−0.87	6.84
BN−$COCl_2$ (**G1**)	−7.53	−4.81	−2.09	5.43
BN−$COCl_2$ (**G2**)	−7.62	−4.82	−2.02	5.59
BN−$COCl_2$ (**G3**)	−7.58	−4.72	−1.87	5.72
Cu−BN (**A1**)	−4.85	−3.29	−1.72	3.13
Cu−BN−$COCl_2$ (**B1**)	−4.87	−3.41	−1.97	2.87
Cu−BN (**A2**)	−4.89	−3.36	−1.83	3.05
Cu−BN−$COCl_2$ (**B2**)	−4.78	−3.64	−2.50	2.28

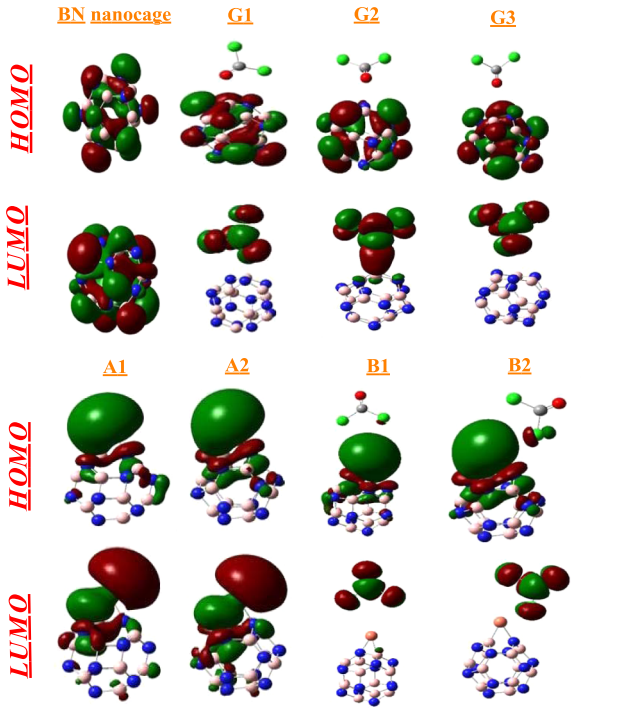

Figure 6. Side views of the HOMO and LUMO of different systems. The isosurface value is 0.02 e/Å^3.

The HOMO−LUMO gap (E_g) is directly related to conductivity,[70] and this relationship is given in the following equation causing a high energy level for the newly formed HOMO.[46,47] According to calculations, the LUMO energies are decreased in **A1** and **A2** geometries as compared to that of the pure BN cage. A change is seen after the adsorption of gas ($COCl_2$) on the Cu-doped BN nanocages. The adsorption of $COCl_2$ on Cu-decorated BN slightly stabilizes the HOMO (except **B2**) and LUMO, where the HOMO−LUMO gaps are 2.87 eV (**B1**) and 2.28 eV (**B2**). The Fermi levels are −3.41 and −3.64 eV for **B1** and **B2** geometries, respectively. Adsorption of phosgene on Cu decreases the interaction of

https://dx.doi.org/10.1021/acsomega.0c00507
ACS Omega 2020, 5, 7641−7650

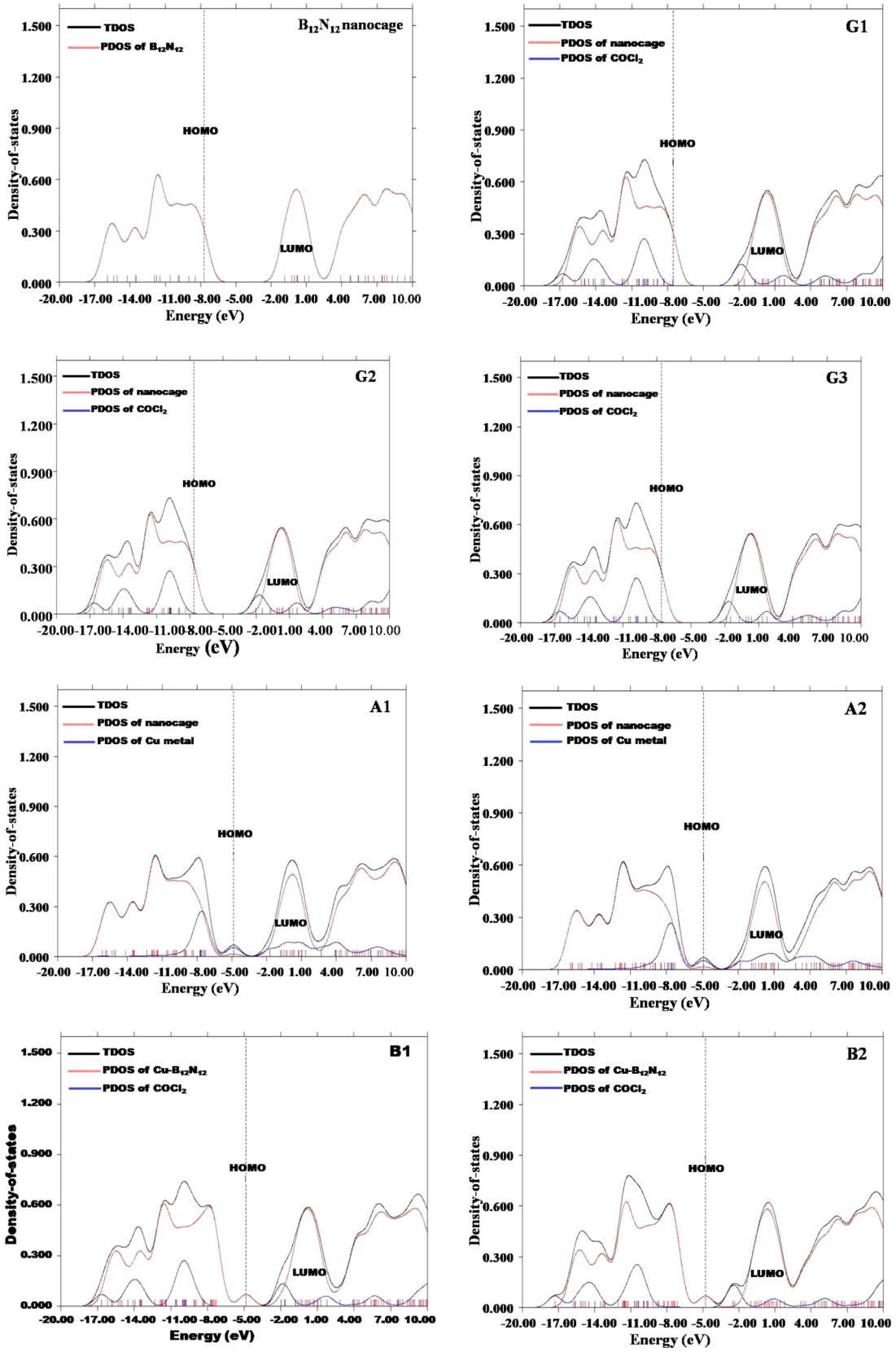

Figure 7. Different systems with their TDOS and PDOS graphs. The isosurface value is 0.02 e/Å^3.

Cu with the BN nanocage. Due to the decrease in coordination to the metal center, the push of the outer d electrons also decreases. The HOMO of $COCl_2$−Cu−BN has more density on the metal and some density on the cage (which is in diffuse form in the cage). The energies of the LUMO are also decreased upon adsorption of $COCl_2$. The shifting of the LUMO on the nanocage causes stabilization of the LUMO by decrease in the energy of LUMO.

https://dx.doi.org/10.1021/acsomega.0c00507
ACS Omega 2020, 5, 7641−7650

$$\sigma \propto \exp(-E_g/KT) \quad (8)$$

This equation indicates the significant increase in electrical conductivity by the decrease in the H−L energy gap (E_g). Based on our findings, it is clearly evident that the sensing ability of the Cu-decorated BN nanocage toward phosgene ($COCl_2$) adsorption is significantly enhanced in comparison with the pristine BN nanocage.

3.6. Partial Density of States. Partial density of states (PDOS) were analyzed to examine the structural changes and electronic properties of BN and Cu−BN nanocages after $COCl_2$ adsorption (with the help of TDOS and PDOS). In the three different orientations (**G1, G2**, and **G3**) of $COCl_2$ on the BN nanocage (Figure 7), the LUMO has density primarily localized on $COCl_2$, whereas the HOMO is centered only on the BN nanocage. For Cu−BN systems, the LUMO is localized on the Cu metal, and the HOMO is merely located on the Cu metal. Upon adsorption of $COCl_2$ on Cu−BN, slightly different results are obtained. In **B1** and **B2** geometries, the LUMO is distributed just on $COCl_2$, whereas the HOMO is present only on Cu−BN. So, from the above discussion, it is clear that shifting of charge density takes place upon adsorption of $COCl_2$ on Cu-doped $B_{12}N_{12}$.

3.7. Global Indices of Reactivity. The effect of $COCl_2$ adsorption on pure and copper-decorated BN cages is also calculated from global indices of reactivity. The properties such as ionization potential (I), electron affinity (A), chemical hardness (η), softness (S), chemical potential (μ), and electrophilicity (ω) are given in Table 3. Here, the ionization potential is the negative of the energy of the HOMO, whereas the electron affinity is the negative of the energy of the LUMO. Generally, the electron-accepting nature of a system is represented with positive values of electron affinity. All systems studied here exhibit good electron-accepting ability, which is a good feature for a system participating in charge-transfer reactions. Similarly, the ionization potential explains the electron-donating ability of a system. Pure $B_{12}N_{12}$ has a high ionization potential value (7.71 eV), which increases upon the interaction of $COCl_2$ on the BN cage (**G1, G2**, and **G3** orientations), but decreases comparatively for copper-decorated BN cages (**A1** and **A2** geometries). The ionization potential again increases after the adsorption of $COCl_2$ on copper-decorated BN nanocages (**B1** and **B2**). A similar trend is observed for electron affinity. Therefore, both properties suggest that our copper-decorated systems are efficient for $COCl_2$ adsorption. Electrophilicity is related to the chemical reactivity of a compound. The pure $B_{12}N_{12}$ cage has an electrophilicity of 2.70 eV, and this property increases in copper-decorated BN nanocages (3.45 eV for **A1** and 3.76 eV for **A2**). The highest value of electrophilicity is calculated for adsorption of $COCl_2$ on copper-decorated $B_{12}N_{12}$ nanocages (4.04 eV for **B1** and 5.81 eV for **B2**). So, the electrophilic index again suggests that our copper-decorated BN systems are best candidates for $COCl_2$ adsorption. The chemical hardness and softness of a compound are directly related to the chemical stability (low reactivity). All our systems are hard in nature with a low value of global softness. The value of chemical potential μ shows a direct relation with the chemical stability and an inverse relation with the reactivity of the system. The chemical potential values suggest that $COCl_2$-adsorbed copper-decorated BN nanocages are more stable with lower reactivity [**B1** (μ = 3.41 eV) and **B2** (μ = 3.64 eV)] as compared to **A1** (μ = 3.29 eV) and **A2** (μ = 3.36 eV). So, all above-mentioned findings suggest that our phosgene-adsorbed copper-decorated systems are stable, least reactive, and best candidates for sensing materials.

Table 3. Ionization Potential (I), Electron Affinity (A), Chemical Hardness (η), Chemical Potential (μ), Softness (S), and Electrophilicity (ω) of Different Systems

systems	I (eV)	A (eV)	η (eV)	μ (eV)	S (eV^{-1})	ω (eV)
Cu	5.98	0.67	2.66	−3.33	0.19	2.08
BN	7.71	0.87	3.42	−4.29	0.15	2.70
BN−$COCl_2$ (**G1**)	7.53	2.09	2.72	−4.81	0.18	4.25
BN−$COCl_2$ (**G2**)	7.62	2.02	2.80	−4.82	0.18	4.15
BN−$COCl_2$ (**G3**)	7.58	1.87	2.86	−4.73	0.18	3.91
Cu−BN (**A1**)	4.85	1.72	1.57	−3.29	0.32	3.45
Cu−BN−$COCl_2$ (**B1**)	4.84	1.97	1.44	−3.41	0.35	4.04
Cu−BN (**A2**)	4.89	1.83	1.53	−3.36	0.33	3.76
Cu−BN−$COCl_2$ (**B2**)	4.78	2.50	1.14	−3.64	0.44	5.81

4. CONCLUSIONS

In this study, we applied the B3LYP/6-31G(d,p) basis set (DFT) to explore phosgene ($COCl_2$) adsorption on pure and Cu-decorated $B_{12}N_{12}$ nanocages. All possible sites on the nanocages are investigated for copper interaction. Two optimized geometries, named Cu@b_{66} (**A1**) and Cu@b_{64} (**A2**), were observed after placing Cu on BN. The binding energy value of **A2** is remarkably higher than that of **A1**, which suggests the enhanced adsorption capability of the BN nanocage toward the $COCl_2$ molecule after Cu decoration. It is evident that $COCl_2$ is more strongly adsorbed on Cu−$B_{12}N_{12}$ as compared to $COCl_2$ when it is exclusively adsorbed on pure $B_{12}N_{12}$. Significant modifications in the electronic properties are observed in $B_{12}N_{12}$ by decoration of Cu and $COCl_2$. Q_{NBO} and dipole moment for the selected systems are indicative of higher charge separation after adsorption of $COCl_2$ on Cu−$B_{12}N_{12}$, as compared to Cu-doped $B_{12}N_{12}$. Dipole moment and Q_{NBO} trends correlate with each other for all systems. The HOMO−LUMO gap of pure BN is higher than those of all other geometries. $COCl_2$ adsorption on pure $B_{12}N_{12}$ and Cu-decorated BN increases the electrophilicity of the $B_{12}N_{12}$ nanocage. Moreover, the partial density of states (PODs) and electronic energy level were calculated to show the effect of Cu and $COCl_2$ decoration on $B_{12}N_{12}$ and Cu−$B_{12}N_{12}$ nanocages, respectively. The results propose the copper-decorated nanocage as an efficient sensor of phosgene and its industrial application in multiple areas.

■ ASSOCIATED CONTENT

Supporting Information

The Supporting Information is available free of charge at https://pubs.acs.org/doi/10.1021/acsomega.0c00507.

Dipole moment vector representation in all systems; Optimized Cartesian coordinates of all geometries (PDF)

■ AUTHOR INFORMATION

Corresponding Author

Khurshid Ayub − *Department of Chemistry, COMSATS University, Abbottabad 22060, Pakistan;* orcid.org/0000-

https://dx.doi.org/10.1021/acsomega.0c00507
ACS Omega 2020, 5, 7641−7650

0003-0990-1860; Phone: +92-992-383591;
Email: Khurshid@cuiatd.edu.pk; Fax: +92-992-383441

Authors

Shahid Hussain − *Department of Applied Chemistry, Government College University, Faisalabad 38000, Pakistan*
Riaz Hussain − *Department of Chemistry, University of Okara, Okara 56300, Pakistan*
Muhammad Yasir Mehboob − *Department of Chemistry, University of Okara, Okara 56300, Pakistan*
Shahzad Ali Shahid Chatha − *Department of Applied Chemistry, Government College University, Faisalabad 38000, Pakistan*
Abdullah Ijaz Hussain − *Department of Applied Chemistry, Government College University, Faisalabad 38000, Pakistan*
Ali Umar − *Department of Chemistry, University of Okara, Okara 56300, Pakistan*
Muhammad Usman Khan − *Department of Applied Chemistry, Government College University, Faisalabad 38000, Pakistan; Department of Chemistry, University of Okara, Okara 56300, Pakistan*
Mahmood Ahmed − *Renacon Pharma (PVT) Limited, Lahore 54600, Pakistan*
Muhammad Adnan − *College of Natural Sciences, Department of Chemistry, Chosun University, Gwangju 501-759, Republic of Korea*

Complete contact information is available at:
https://pubs.acs.org/10.1021/acsomega.0c00507

Notes

The authors declare no competing financial interest.

■ ACKNOWLEDGMENTS

The authors acknowledge the financial and technical support from the Shakarganj Limited Company, Jhang, Punjab, Pakistan.

■ REFERENCES

(1) Iijima, S. Helical Microtubules of Graphitic Carbon. *Nature* **1991**, *354*, 56−58.
(2) Mias, S.; Sudor, J.; Camon, H. PNIPAM: A Thermo-Activated Nano-Material for Use in Optical Devices. *Microsyst. Technol.* **2008**, *14*, 747−751.
(3) Gu, M.; Zhang, Q.; Lamon, S. Nanomaterials for Optical Data Storage. *Nat. Rev. Mater.* **2016**, *1*, No. 16070.
(4) Planeix, J. M.; Coustel, N.; Coq, B.; Brotons, V.; Kumbhar, P. S.; Dutartre, R.; Geneste, P.; Bernier, P.; Ajayan, P. M. Application of Carbon Nanotubes as Supports in Heterogeneous Catalysis. *J. Am. Chem. Soc.* **1994**, *116*, 7935−7936.
(5) Varghese, S. S.; Lonkar, S.; Singh, K. K.; Swaminathan, S.; Abdala, A. Recent Advances in Graphene Based Gas Sensors. *Sensor. Actuators, B* **2015**, *218*, 160−183.
(6) Rad, A. S.; Shabestari, S. S.; Mohseni, S.; Aghouzi, S. A. Study on the Adsorption Properties of O 3, SO 2, and SO 3 on B-Doped Graphene Using DFT Calculations. *J. Solid State Chem.* **2016**, *237*, 204−210.
(7) Rad, A. S.; Ayub, K. Ni Adsorption on Al12P12 Nano-Cage: A DFT Study. *J. Alloys Compd.* **2016**, *678*, 317−324.
(8) Qiang, Y.; Antony, J.; Sharma, A.; Nutting, J.; Sikes, D.; Meyer, D. Iron/Iron Oxide Core-Shell Nanoclusters for Biomedical Applications. *J. Nanopart. Res.* **2006**, *8*, 489−496.
(9) Talla, J. A. Ab Initio Simulations of Doped Single-Walled Carbon Nanotube Sensors. *Chem. Phys.* **2012**, *392*, 71−77.
(10) Chopra, N. G.; Luyken, R. J.; Cherrey, K.; Crespi, V. H.; Cohen, M. L.; Louie, S. G.; Zettl, A. Boron Nitride Nanotubes. *Science* **1995**, *269*, 966−967.
(11) Han, W.; Bando, Y.; Kurashima, K.; Sato, T. Synthesis of Boron Nitride Nanotubes from Carbon Nanotubes by a Substitution Reaction. *Appl. Phys. Lett.* **1998**, *73*, 3085−3087.
(12) Sun, X.-H.; Li, C.-P.; Wong, W.-K.; Wong, N.-B.; Lee, C.-S.; Lee, S.-T.; Teo, B.-K. Formation of Silicon Carbide Nanotubes and Nanowires via Reaction of Silicon (from Disproportionation of Silicon Monoxide) with Carbon Nanotubes. *J. Am. Chem. Soc.* **2002**, *124*, 14464−14471.
(13) Wu, Q.; Hu, Z.; Wang, X.; Lu, Y.; Chen, X.; Xu, H.; Chen, Y. Synthesis and Characterization of Faceted Hexagonal Aluminum Nitride Nanotubes. *J. Am. Chem. Soc.* **2003**, *125*, 10176−10177.
(14) Haberland, H.; Ludewigt, C.; Richter, T. Electron Attachment to Clusters Composed of Closed Shell, Hydrogen Containing Molecules. *Z. Phys. D: At., Mol. Clusters* **1989**, *12*, 289−290.
(15) Jensen, F.; Toftlund, H. Structure and Stability of C24 and B12N12 Isomers. *Chem. Phys. Lett.* **1993**, *201*, 89−96.
(16) Strout, D. L. Structure and Stability of Boron Nitrides: Isomers of B 12 N 12. *J. Phys. Chem. A* **2000**, *104*, 3364−3366.
(17) Kandalam, A. K.; Blanco, M. A.; Pandey, R. Theoretical Study of AlnNn, GanNn, and InnNn (n = 4, 5, 6) Clusters. *J. Phys. Chem. B* **2002**, *106*, 1945−1953.
(18) Costales, A.; Kandalam, A. K.; Franco, R.; Pandey, R. Theoretical Study of Structural and Vibrational Properties of (AlP) n, (AlAs) n, (GaP) n, (GaAs) n, (InP) n, and (InAs) n Clusters with n = 1, 2, 3. *J. Phys. Chem. B* **2002**, *106*, 1940−1944.
(19) Paine, R. T.; Narula, C. K. Synthetic Routes to Boron Nitride. *Chem. Rev.* **1990**, *90*, 73−91.
(20) Maria; Iqbal, J.; Ludwig, R.; Ayub, K. Phosphides or Nitrides for Better NLO Properties? A Detailed Comparative Study of Alkali Metal Doped Nano-Cages. *Mater. Res. Bull.* **2017**, *92*, 113−122.
(21) Oku, T.; Kuno, M.; Kitahara, H.; Narita, I. Formation, Atomic Structures and Properties of Boron Nitride and Carbon Nanocage Fullerene Materials. *Int. J. Inorg. Mater.* **2001**, *3*, 597−612.
(22) Oku, T.; Nishiwaki, A.; Narita, I. Formation and Atomic Structure of B 12 N 12 Nanocage Clusters Studied by Mass Spectrometry and Cluster Calculation. *Sci. Technol. Adv. Mater.* **2004**, *5*, 635−638.
(23) Oku, T.; Hirano, T.; Kuno, M.; Kusunose, T.; Niihara, K.; Suganuma, K. Synthesis, Atomic Structures and Properties of Carbon and Boron Nitride Fullerene Materials. *Mater. Sci. Eng. B* **2000**, *74*, 206−217.
(24) Esrafili, M. D.; Nurazar, R. Methylamine Adsorption and Decomposition on B12N12 Nanocage: A Density Functional Theory Study. *Surf. Sci.* **2014**, *626*, 44−48.
(25) Beheshtian, J.; Baei, M. T.; Peyghan, A. A. Theoretical Study of CO Adsorption on the Surface of BN, AlN, BP and AlP Nanotubes. *Surf. Sci.* **2012**, *606*, 981−985.
(26) Baei, M. T.; Peyghan, A. A.; Bagheri, Z. A. DFT Study on CO 2 Interaction with a BN Nano-Cage. *Bull. Korean Chem. Soc.* **2012**, *33*, 3338−3342.
(27) Beheshtian, J.; Peyghan, A. A.; Bagheri, Z.; Kamfiroozi, M. Interaction of Small Molecules (NO, H2, N2, and CH4) with BN Nanocluster Surface. *Struct. Chem.* **2012**, *23*, 1567−1572.
(28) Rad, A. S.; Ayub, K. Adsorption of Thiophene on the Surfaces of X 12 Y 12 (X = Al, B, and Y = N,P) Nanoclusters; A DFT Study. *J. Mol. Liq.* **2017**, *238*, 303−309.
(29) Rad, A. S. Application of B12N12 and B12P12 as Two Fullerene-like Semiconductors for Adsorption of Halomethane: Density Functional Theory Study. *Semiconductors* **2017**, *51*, 134−138.
(30) Rad, A. S.; Ayub, K. O 3 and SO 2 Sensing Concept on Extended Surface of B 12 N 12 Nanocages Modified by Nickel Decoration: A Comprehensive DFT Study. *Solid State Sci.* **2017**, *69*, 22−30.
(31) Muhammad, S.; Janjua, M. R. S. A.; Su, Z. Investigation of Dibenzoboroles Having π-Electrons: Toward a New Type of Two-

Dimensional NLO Molecular Switch? *J. Phys. Chem. C* **2009**, *113*, 12551−12557.
(32) Muhammad, S.; Xu, H.; Janjua, M. R. S. A.; Su, Z.; Nadeem, M. Quantum Chemical Study of Benzimidazole Derivatives to Tune the Second-Order Nonlinear Optical Molecular Switching by Proton Abstraction. *Phys. Chem. Chem. Phys.* **2010**, *12*, 4791.
(33) Muhammad, S.; Liu, C.; Zhao, L.; Wu, S.; Su, Z. A Theoretical Investigation of Intermolecular Interaction of a Phthalimide Based "On−off" Sensor with Different Halide Ions: Tuning Its Efficiency and Electro-Optical Properties. *Theor. Chem. Acc.* **2009**, *122*, 77−86.
(34) Muhammad, S.; Minami, T.; Fukui, H.; Yoneda, K.; Kishi, R.; Shigeta, Y.; Nakano, M. Halide Ion Complexes of Decaborane (B 10 H 14) and Their Derivatives: Noncovalent Charge Transfer Effect on Second-Order Nonlinear Optical Properties. *J. Phys. Chem. A* **2012**, *116*, 1417−1424.
(35) Esrafili, M. D.; Nurazar, R. A Density Functional Theory Study on the Adsorption and Decomposition of Methanol on B12N12 Fullerene-like Nanocage. *Superlattices Microstruct.* **2014**, *67*, 54−60.
(36) Baei, M. T.; Taghartapeh, M. R.; Lemeski, E. T.; Soltani, A. A Computational Study of Adenine, Uracil, and Cytosine Adsorption upon AlN and BN Nano-Cages. *Phys. B* **2014**, *444*, 6−13.
(37) Rad, A. S.; Ayub, K. A Comparative Density Functional Theory Study of Guanine Chemisorption on Al12N12, Al12P12, B12N12, and B12P12 Nano-Cages. *J. Alloys Compd.* **2016**, *672*, 161−169.
(38) Soltani, A.; Baei, M. T.; Lemeski, E. T.; Pahlevani, A. A. The Study of SCN − Adsorption on B 12 N 12 and B 16 N 16 Nano-Cages. *Superlattices Microstruct.* **2014**, *75*, 716−724.
(39) Rad, A. S.; Ayub, K. Enhancement in Hydrogen Molecule Adsorption on B 12 N 12 Nano-Cluster by Decoration of Nickel. *Int. J. Hydrogen Energy* **2016**, *41*, 22182−22191.
(40) Rad, A. S.; Ayub, K. Adsorption of Pyrrole on Al12N12, Al12P12, B12N12, and B12P12 Fullerene-like Nano-Cages; a First Principles Study. *Vacuum* **2016**, *131*, 135−141.
(41) Oku, T.; Narita, I. Calculation of H2 Gas Storage for Boron Nitride and Carbon Nanotubes Studied from the Cluster Calculation. *Phys. B* **2002**, *323*, 216−218.
(42) Oku, T.; Kuno, M. Synthesis, Argon/Hydrogen Storage and Magnetic Properties of Boron Nitride Nanotubes and Nanocapsules. *Diam. Relat. Mater.* **2003**, *12*, 840−845.
(43) Ayub, K. Transportation of Hydrogen Atom and Molecule through X 12 Y 12 Nano-Cages. *Int. J. Hydrogen Energy* **2017**, *42*, 11439−11451.
(44) Ayub, K. Binding Affinity and Permeation of X12Y12 Nanoclusters for Helium and Neon. *J. Mol. Liq.* **2017**, *244*, 124−134.
(45) Radosavljević, M.; Appenzeller, J.; Derycke, V.; Martel, R.; Avouris, P.; Loiseau, A.; Cochon, J.-L.; Pigache, D. Electrical Properties and Transport in Boron Nitride Nanotubes. *Appl. Phys. Lett.* **2003**, *82*, 4131−4133.
(46) Ayub, K. Are Phosphide Nano-Cages Better than Nitride Nano-Cages? A Kinetic, Thermodynamic and Non-Linear Optical Properties Study of Alkali Metal Encapsulated X 12 Y 12 Nano-Cages. *J. Mater. Chem. C* **2016**, *4*, 10919−10934.
(47) Maria; Iqbal, J.; Ayub, K. Enhanced Electronic and Non-Linear Optical Properties of Alkali Metal (Li, Na, K) Doped Boron Nitride Nano-Cages. *J. Alloys Compd.* **2016**, *687*, 976−983.
(48) Tokoro, H.; Fujii, S.; Oku, T. Iron Nanoparticles Coated with Boron Nitride Nanolayers Synthesized by a Solid Phase Reaction. *IEEE Trans. Magn.* **2003**, *39*, 2761−2763.
(49) Xie, W.; Wang, J.; Wang, J.; Wu, X.; Wang, Z.; Zhang, R.-Q. High-Angular-Momentum Orbitals and Superatomic Characteristics of Boron-Nitrogen Cages. *J. Phys. Chem. C* **2020**, *124*, 3881−3885.
(50) Munsif, S.; Ayub, K. Diffusion of Alkali Metal Atoms (Li, Na, K) on Aluminum Nitride and Boron Nitride Nanocages; a Density Functional Theory Study. *J. Mol. Liq.* **2018**, *259*, 249−259.
(51) Munsif, S.; Ayub, K. Permeability and Storage Ability of Inorganic X 12 Y 12 Fullerenes for Lithium Atom and Ion. *Chem. Phys. Lett.* **2018**, *698*, 51−59.
(52) Grainge, C.; Rice, P. Management of Phosgene-Induced Acute Lung Injury. *Clin. Toxicol.* **2010**, *48*, 497−508.
(53) Shahabi, M.; Raissi, H. Molecular Dynamics Simulation and Quantum Chemical Studies on the Investigation of Aluminum Nitride Nanotube as Phosgene Gas Sensor. *J. Inclusion Phenom. Macrocyclic Chem.* **2016**, *86*, 305−322.
(54) Dole, M. The Rate of Adsorption of Phosgene and Chloropicrin on Charcoal. *J. Chem. Phys.* **1947**, *15*, 447−454.
(55) Joung, S.-K.; Amemiya, T.; Murabayashi, M.; Cai, R.; Itoh, K. Chemical Adsorption of Phosgene on TiO2 and Its Effect on the Photocatalytic Oxidation of Trichloroethylene. *Surf. Sci.* **2005**, *598*, 174−184.
(56) Beheshtian, J.; Peyghan, A. A.; Bagheri, Z. Detection of Phosgene by Sc-Doped BN Nanotubes: A DFT Study. *Sens. Actuators, B* **2012**, *171−172*, 846−852.
(57) Shakerzadeh, E.; Khodayar, E.; Noorizadeh, S. Theoretical Assessment of Phosgene Adsorption Behavior onto Pristine, Al- and Ga-Doped B 12 N 12 and B 16 N 16 Nanoclusters. *Comput. Mater. Sci.* **2016**, *118*, 155−171.
(58) Padash, R.; Rahimi-Nasrabadi, M.; Rad, A. S.; Sobhani-Nasab, A.; Jesionowski, T.; Ehrlich, H. A Comparative Computational Investigation of Phosgene Adsorption on (XY)12 (X = Al, B and Y = N, P) Nanoclusters: DFT Investigations. *J. Clust. Sci.* **2018**, *30*, 203−218.
(59) Abbasi, M.; Nemati-Kande, E.; Mohammadi, M. D. Doping of the First Row Transition Metals onto B 12 N 12 Nanocage: A DFT Study. *Comput. Theor. Chem.* **2018**, *1132*, 1−11.
(60) Wimmer, E.; Fu, C. L.; Freeman, A. J. Catalytic Promotion and Poisoning: All-Electron Local-Density-Functional Theory of CO on Ni(001) Surfaces Coadsorbed with K or S. *Phys. Rev. Lett.* **1985**, *55*, 2618−2621.
(61) Yates, J. T.; Garland, C. W. Infrared Studies of Carbon Monoxide Chemisorbed on Nickel And on Mercury-poisoned Nickel Surfaces 1. *J. Phys. Chem. A.* **1961**, *65*, 617−624.
(62) Imanaka, T.; Nitta, Y.; Teranishi, S. Study of the Poisoning Effect on Nickel and Nickel Boride Catalysts by Means of a Flow Microcalorimeter. *Bull. Chem. Soc. Jpn.* **1973**, *46*, 1134−1136.
(63) Rad, A. S.; Ayub, K. How Can Nickel Decoration Affect H 2 Adsorption on B 12 P 12 Nano-Heterostructures? *J. Mol. Liq.* **2018**, *255*, 168−175.
(64) Rad, A. S.; Ayub, K. Enhancement in Hydrogen Molecule Adsorption on B12N12 Nano-Cluster by Decoration of Nickel. *Int. J. Hydrogen Energy* **2016**, *41*, 22182−22191.
(65) Frisch, M.; Trucks, G.; Schlegel, H. B.; Scuseria, G. E.; Robb, M. A.; Cheeseman, J. R.; Scalmani, G.; Barone, V.; Mennucci, B.; Petersson, G. A. et al.. *Gaussian 09*, revision A. 02; Gaussian. Inc.: Wallingford, CT, 2009. 200 (11 june 2009).
(66) Hussain, S.; Chatha, S. A. S.; Hussain, A. I.; Hussain, R.; Mehboob, M. Y.; Muhammad, S.; Ahmad, Z.; Ayub, K. Zinc-Doped Boron Phosphide Nanocluster as Efficient Sensor for SO2. *J. Chem.* **2020**, 1−12.
(67) Parr, R. G.; Szentpály, L.V.; Liu, S. Electrophilicity Index. *J. Am. Chem. Soc.* **1999**, *121*, 1922−1924.
(68) Pearson, R. G. The Transition Metal-Carbon Monoxide Bond. *Inorg. Chem.* **1984**, *23*, 4675−4679.
(69) Lu, T.; Chen, F. Multiwfn: A Multifunctional Wavefunction Analyzer. *J. Comput. Chem.* **2012**, *33*, 580−592.
(70) Li, S. S. Scattering Mechanisms and Carrier Mobilities in Semiconductors. In *Semiconductor Physical Electronics*; Springer: New York, NY, pp 211−245.

https://dx.doi.org/10.1021/acsomega.0c00507
ACS Omega 2020, 5, 7641−7650